Optical spectroscopy and scintillation mechanisms of $Ce_xLa_{1-x}F_3$

A. J. Wojtowicz,* M. Balcerzyk,* E. Berman, and A. Lempicki
Department of Chemistry, Boston University, 590 Commonwealth Avenue, Boston, Massachusetts 02215
and ALEM Associates, 303A Commonwealth Avenue, Boston, Massachusetts 02115
(Received 2 July 1993; revised manuscript received 6 December 1993)

In this paper we present spectroscopic and scintillation studies of mixed cerium lanthanum trifluoride crystals $Ce_xLa_{1-x}F_3$. A scintillation mechanism is proposed in which the light output of the $Ce_xLa_{1-x}F_3$ scintillator is determined by three processes: a direct excitation of Ce^{3+} ions by secondary electrons and x rays, an ionization of Ce^{3+} ions followed by the capture of electrons and formation of Ce bound excitons and, eventually, a transfer of the energy from the electronic-lattice excitations to Ce^{3+} ions. These three processes occur in various degrees in *all* inorganic Ce scintillators, and the mixed (Ce,La) trifluorides provide, therefore, an excellent example of their relative importance. The peculiarity of fluorides is that Ce^{3+} ions occur in regular and "perturbed" sites. The lack of a fast energy migration between the Ce ions and, at the same time, an efficient energy transfer to "perturbed" Ce ions lead to nonexponential decays of the Ce emission. Thermal quenching is moderate and radiation trapping can be minimized, and there is no evidence of luminescence concentration quenching. The light output under γ excitation has a maximum value of about 4500 photons per MeV, which is significantly lower than the estimated conversion-limited value of about 25 000 photons per MeV. It is suggested that the stable Ce^{2+} provides electron traps, competing for electrons with holes localized on F_2^- and Ce^{4+} ions. Therefore, mostly one process, namely the direct excitation of Ce^{3+} ions by secondary electrons and photons, contributes to the light output of CeF_3. The deomonstrated feasibility of reducing perturbed Ce makes it a strong contender in those applications where high speed, not high light output, is of prime concern.

I. INTRODUCTION

Broadband, efficient, and rapidly decaying emissions characteristic of parity-allowed d-f transitions of rare-earth (R) ions have played an important role in solid-state spectroscopy for the past three decades. Lower-lying $4f^{n-1}5d \leftrightarrow 4f^n$ transitions on R^{2+} ions found important applications in both phosphors,[1] and lasers.[2] Higher energy $4f^{n-1}5d \rightarrow 4f^n$ transitions in R^{3+} ions are characterized by significantly shorter decay times,[3] which promote applications requiring high speed, such as flying spot scanners or beam-indexing phosphors. However, only three ions (Ce^{3+}, Pr^{3+}, and Th^{3+}), have their first excited d state below the 55 000 cm^{-1} ultraviolet cutoff in the air.[4] Of those, the Ce^{3+} ion has been broadly used as an activator in phosphors,[5] and, together with the Pr^{3+}, was considered for laser applications.[6] Eventually, lasing was demonstrated in the case of Ce.[7]

Today the area of large bandgap materials activated with R^{3+} is once again attracting the attention of researchers. Most of this renewed interest is driven by new applications in science, medicine, and industry that require faster and more efficient scintillation detectors (see, e.g., Ref. 8). In high-energy physics, BaF_2 was considered for the superconducting supercollider[9] and CeF_3 is a strong candidate for the new calorimeter at CERN (130 000 monocrystals, total volume of about 60 m^3).[10] In medical applications, positron emission tomography (PET) currently utilizes slower scintillators ($Bi_4Ge_3O_{12}$—BGO, or Tl-doped halides). The future of PET is tied to faster and at least equally efficient scintillators.[11]

While it has been recognized, that for scintillators a fast decay and a high quantum efficiency of the activator ion are important factors to be considered,[12] much less attention has been paid to the processes by which the energy carried by a high-energy particle is converted and transferred to the emitting ions. Conversion results in generation of electronic-lattice excitations (electron-hole pairs and/or excitons) and is measured by the number of such excitations per unit incident energy. In the next step an efficient transfer of these excitations to luminescing ions is necessary. As discussed by Lempicki, Wojtowicz, and Berman,[13] both steps are critical for the overall performance (efficiency and speed) of the scintillator.

The efficiency of energy transfer from lattice excitations to the rare-earth dopants can be assessed from luminescence excitation spectra. In their study of Nd^{3+}, Er^{3+}, and Tm^{3+} ions in trifluorides, Yang and DeLuca found a significant difference between excitation spectra of inter- ($5d^14f^{n-1} \rightarrow 4f^n$) and intraconfigurational ($4f^n \rightarrow 4f^n$) luminescent transitions.[14] The presence of the strong excitation peak at the energy of the band-to-band transition in excitation spectra of the lower energy f-f emissions suggests that an efficient transfer from lattice excitations is possible. Curiously enough, this peak is totally absent in excitation spectra of d-f transitions, presumably because the large relaxation of lattice excitations prevents them from being efficiently transferred to the higher-energy d-f transitions.[14] Therefore in the scintillation spectra under ionizing excitation the parity forbidden f-f transitions prevail over the allowed d-f transitions, a peculiar and rather unexpected result.[15]

Since d levels of Ce^{3+} ion are known to be the lowest among all trivalent R^{3+},[4] it is reasonable to expect that, for this ion, the lattice-to-activator energy transfer may contribute to the excitation of d-f transitions. This is confirmed by the excitation spectra of Ce^{3+} luminescence in LuF_3 (Ref. 4) and LaF_3,[16] which clearly show bands due to both f-d and band-to-band transitions. One is therefore led to believe that adequately high Ce doping is likely to produce a scintillator with light output limited only by the conversion efficiency and characterized by the high speed of the allowed, d-f transition on the Ce^{3+} ion. Should no detrimental effects due to high concentrations of Ce be observed, one would expect stoichiometric Ce compounds to be ideal candidates for fast and efficient scintillators. This hypothesis was severely shaken by the observation that two stoichiometric Ce materials studied so far, namely CeF_3 and CeP_5O_{14}, show light outputs much lower than their calculated conversion would indicate.[13] Evidently high concentration, decent conversion, and high quantum efficiency are not sufficient conditions for high scintillation light output.[17,18]

The CeF_3 scintillator, discovered independently by Anderson,[19] and Moses and Derenzo,[20] created a lot of interest, especially since it showed an ultrafast (2–5 ns) component in its scintillation decay.[21] However, it was proved later that this component is not due to any separate process but results from a quenching of the Ce emission.[17] The light output was found to be disappointingly low and the spectroscopy of CeF_3 proved to be complex, clearly indicating presence of "perturbed" Ce sites.[17] Nevertheless, significant improvements were expected, based on the assumption that the loss in the Ce emission was nonradiative and that the "perturbed" Ce ions (Ce_{per}) were efficiently competing with the regular Ce ions for the energy deposited in the lattice.[17] However, it was also suggested that the Ce_{per} ions might be fed by a nonradiative energy transfer from the regular Ce ions.[17,22] If so, there would be no obvious reason for a significant loss in the combined light output. Despite this, processes resulting from presence of the Ce_{per} ions are undesirable because they invariably lead to changes in intensities, spectra, and decay times along the length of larger crystals required by some applications. The constant and significant progress made by crystal growers (Optovac) in reducing the level of Ce_{per} in CeF_3 will be documented in this paper. Eventually these efforts are likely to produce a superior material for applications in high-energy physics.

The low light output of both CeF_3 and Ce pentaphosphate (CeP_5O_{14}) led Wojtowicz, Berman, and Lempicki to propose a model of scintillation mechanism in these materials.[18,23] They observe that in the presence of strong lattice relaxation the conversion process is likely to result in two distinct types of lattice excitations (excitons). In the *first* type the hole is localized on the anion sublattice (fluorine or phosphate group), with the electron bound by the net Coulomb potential of the localized hole (a self-trapped lattice exciton), while in the *second* type the hole is bound by the local potential of Ce^{3+} ion (creating Ce^{4+}), which subsequently binds a conduction electron (Ce bound exciton). While the Ce-bound exciton can efficiently transfer its energy to the d-f structure of Ce^{3+} ion, a larger lattice relaxation may prevent (or retard) such a transfer in the case of self-trapped lattice excitons. The partition of the total energy between these two types of lattice excitations—one useful, one useless—was expected to explain the low light outputs of the Ce pentaphosphate and trifluoride scintillators. New results on concentration dependence of the light output of (Ce,La) trifluorides, to be presented and discussed in this paper, require some extension of this model. As we shall see we will have to include a *third* process of direct Ce excitation by secondary electrons and x rays which does not involve electron-hole pairs or excitons. These three processes exhaust all the excitation mechanisms encountered in inorganic Ce-based scintillators.

II. MATERIALS AND EXPERIMENT

LaF_3 and CeF_3 crystals are characterized by the same space group, D_{3d}^4 ($P\bar{3}c1$).[24] The lattice constants are $a=7.13$ Å and $c=7.29$ Å, and there are six molecules in the unit cell.[24] There is only one La (Ce) site of C_2 symmetry and its coordination sphere contains nine F^- ions at distances between 2.42 and 2.64 Å and two others at 2.99 Å.[24] The other La (Ce) ions are at the following distances: about 4.10 Å (six ions), 4.35 Å (six ions), 5.99 Å (six ions), 6.29 Å (four ions), and 7.2 Å (six ions).[24] The density of $Ce_xLa_{1-x}F_3$ crystals is about 6.16 g/cm^3, and the number of cations and anions are 1.88×10^{22} and 5.64×10^{22} ions/cm^3, respectively.[24] The cerium and lanthanum trifluorides are insulators with bandgap energies of about 10.1–10.4 eV.[25] The highest optical phonon energy is about 466 cm^{-1}.[26] The refractive indices of $Ce_xLa_{1-x}F_3$ crystals can be calculated from the following formula:[27]

$$\frac{1}{n^2-1}=\frac{A}{\lambda^2}+B\ , \tag{1}$$

where, from the fit to data of Ref. 27 (averaged between extraordinary and ordinary indices) we substitute: $A=-5075.83-738.15x$ and $B=0.655\,249-0.016\,477x$.

Three sets of $Ce_xLa_{1-x}F_3$ samples were studied. Two of them, marked M and M', were grown at Optovac specifically for the purpose of this study. As starting materials LaF_3 and CeF_3 powders from Rhone-Poulenc, Phoenix, AZ (nominally 99.95% pure) were used. These materials were pretreated using a proprietary method of Optovac. The growth was performed by a Bridgman-Stockbarger method in graphite crucibles using furnace employing graphite heating elements. Crystal growth was done under vacuum with solidification proceeding from the bottom of the melt upwards, by translating the crucibles through the temperature gradient zone spanning the melting point of the material (the pulling rate was about two inches per day). Compositions were controlled by mixing the appropriate amounts of components with 2% (by weight) of Merck Optipur PbF_2, which served as an oxygen scavenger. During the growth process oxygen was evaporated from the sample as PbO. Each sample, of about 44 g, was placed in the individual

graphite crucible and all crucibles were put into the furnace. After the growth was completed the temperature was lowered to about 850 °C and samples were annealed for 24 h. The cooling time was two days for the M set and seven days for the M' set. With the exception of a few control samples all of the samples were cut from the middle of the boules characterized by the best optical properties. Crystals were very clear, with the size of about $8\times6\times5$ mm. The crystals of the third set marked "designation" were also grown at Otovac during the past 10 years. The number of samples and their designations were as follows:

	$x=0$	$x=1$	$0<x<1$
Set M	2	5	18
Set M'		3	12
designation	"H"	"A"–"G"	"J" ($x=0.05$)

All undoped LaF_3 crystals show bright Ce^{3+} photoluminescence due to the inadvertent Ce contamination, presumably in very low concentration.

Luminescence spectra under optical excitation were measured using a right angle geometry. Since there is no selection rule imposed by the C_2 symmetry of the Ce site,[28] the samples were not oriented and no polarizers were used. We have employed a 0.25-m Jarrell-Ash 82–410 monochromator with a 1180 grooves/mm grating blazed at 300 nm. The monochromator was equipped with the Hamamatsu R2059 dry-ice-cooled photomultiplier tube with quartz window. For luminescence excitation spectra a 0.22-m Spex 1680 double monochromator, was used with a Xe lamp. Optically excited decays were measured using the Stanford Research SR270 boxcar averager with a 0.5-ns gate. Excitation was provided by the FL2000 Lambda-Physik dye laser pumped by a N_2 laser operator at 20 Hz and producing pulses of about 3 ns duration time. The dye laser light was frequency doubled using a KDP crystal. In most experiments the sample was mounted on the cold finger of the CTI Cryogenics closed-cycle He cooler, providing variable temperatures between 23 and 600 K. All spectra were corrected for the spectral response of the optical system and are expressed in arbitrary units proportional to the number of transitions per second and per unit wavelength, (photons/s nm). Energy spectra were measured using a standard System 100 Canberra setup and a ^{207}Bi source (0.481, 0.554, 0.976, and 1.048-MeV γ and β radiation). Decays under γ and β excitation (Ru/Rh source), were measured using the same equipment adapted for synchronous photon counting.[29] All experiments were controlled by personal computers where data were stored for subsequent analysis.

Additional experiments were performed at the National Synchrotron Light Source at the Brookhaven National Laboratory which allowed the extension of the excitation wavelength range down to 200 nm. The pulse width and repetition frequency were 0.5 ns and 5.88 MHz, respectively, providing an opportunity of measuring fast rise and decay times under optical excitation.

III. RESULTS

To arrive at meaningful conclusions we examined a large number of samples differing widely in Ce concentration and conditions of growth. Since great progress was made over the years in improving crystal quality there are large differences in their spectral characteristics, as reported earlier.[17,22] In particular early reports (e.g., Ref. 30) show significant distortions in spectra pointing to problems of maintaining crystal purity and quality. It is impractical to present in this paper all the experimental results which have been obtained. Instead we make a selection and present only those which we consider to be the most meaningful and indicative of the basic mechanisms involved.

A. Luminescence spectra

In Fig. 1 we present the room-temperature (RT), steady-state luminescence spectra under optical (250 nm), and ionizing (γ and β) excitations for five crystals of $Ce_xLa_{1-x}F_3$ from set M with x equal to 0.0001, 0.01, 0.1, 0.5, and 1. There is no significant difference between spectra under optical and ionizing excitations. For small x the spectra are dominated by two bands, at 286 and 303 nm, which are due to transitions terminating on the spin-orbit split $^2F_{5/2}$ and $^2F_{7/2}$ states of the f^1 configuration as described earlier.[30] We will designate these two bands short-wavelength luminescence (SWL).

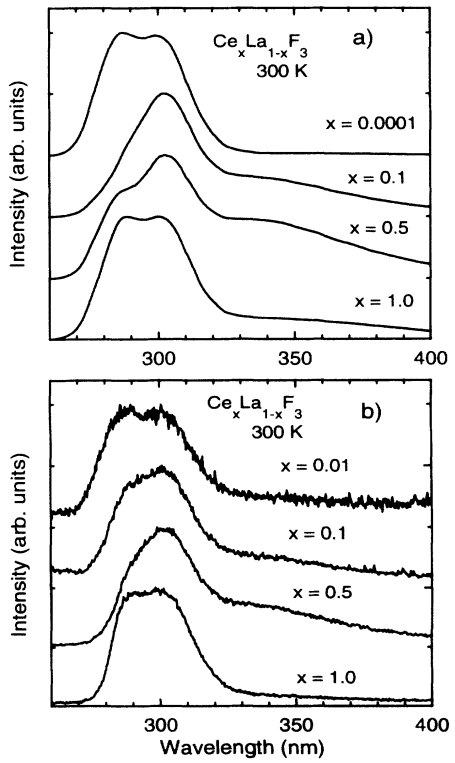

FIG. 1. The room-temperature luminescence spectra of $Ce_xLa_{1-x}F_3$, set M, for various Ce concentrations x. (a) optical excitation at 250 nm, (b) γ and β ionizing excitation, Ru/Rh source.

The third additional band appears at longer wavelengths (340 nm).[30] We will designate it long-wavelength luminescence (LWL). As we shall see the preponderant evidence is that this band is due to a fraction of cerium ions residing in "perturbed" sites as suggested earlier.[17,22] The contribution of the LWL band increases with increasing x, up to 30% of the total luminescence at $x \simeq 0.5-0.6$. For $x \geq 0.7$ the LWL contribution unexpectedly decreases again (to about 10–15 % for $x = 1$) and the spectrum of CeF_3 (sample 24*M*) resembles closely that of LaF_3:Ce (0.01%). As shown in Fig. 2 the spectra of different CeF_3 crystals indicate various contributions of the LWL band, sometimes to the point (sample A) that this band dominates the spectrum. It is interesting to observe that all of the spectra shown in Figs. 1 and 2 clearly indicate that an increase in the relative contribution of the LWL band is accompanied by a decrease of the 286-nm band of the SWL. This is also true of spectra of one crystal taken at different temperatures, as shown in Figs. 3 and 4. The effect is most pronounced for crystals which show significant presence of the LWL such as sample *B*, (compare traces *b*, *c*, and *d* in Fig. 3). The spectra of crystals which show less of the LWL [e.g., CeF_3 from the set *M* or a very diluted Ce case like undoped LaF_3 (H), trace *a* in Fig. 3] do not show changes in distribution of luminescence intensity between the SWL and LWL emissions as a function of temperature. In Fig. 3 the broken lines represent components into which the spectra were decomposed by first transforming the spectra to line-shape functions, fitting them to Gaussian functions and then transforming back to intensity vs wavelength (see e.g., Ref. 31). The spectra of the Ce emission (the SWL band) are reasonably well approximated by Gaussian functions, suggesting a relatively strong electron-lattice coupling. The LWL band could not, however, be reproduced by only one Gaussian function which suggests that this band is inhomogeneously broadened, as reported before.[20,22] The results of this procedure are summarized in Table I.

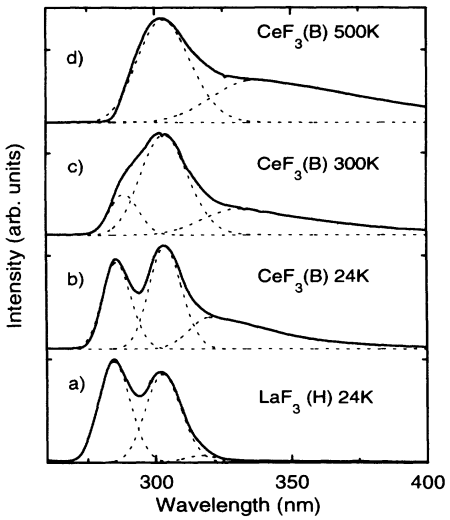

FIG. 3. Luminescence spectra of sample *B* (CeF_3) for different temperatures under optical excitation at 250 nm, (traces *b*, *c*, and *d*). For comparison the spectrum of the sample *H*, nominally undoped LaF_3 at 24 K is also shown (trace *a*). Dashed lines represent the Gaussian functions into which the spectra were decomposed.

B. Luminescence excitation spectra

Figure 5 shows excitation spectra of three emissions of CeF_3 (sample 24*M*) taken at 35 K. Since 286- and 303-nm bands of the SWL originate from the same lowest energy state of the crystal-field split *d* configuration of the Ce^{3+} ion we expect the two upper traces to be similar. The lower trace shows that the LWL excitation characteristic band is clearly shifted to longer wavelengths, as noted before.[17,22] By comparing the position of this band with those of the Ce-emission bands shown in Figs. 1, 2, and 3 we immediately see a large overlap which indicates the possibility of the radiative and nonradiative energy

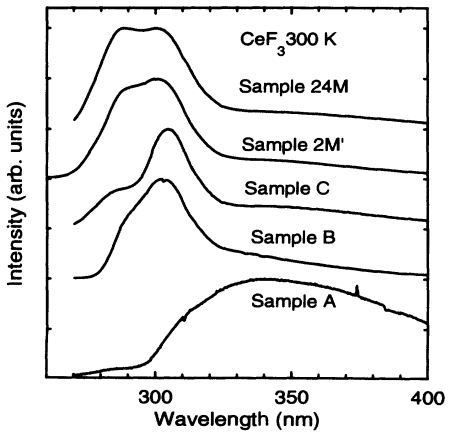

FIG. 2. Comparison of the luminescence spectra of various samples of CeF_3 under optical excitation (250 nm) at room temperature.

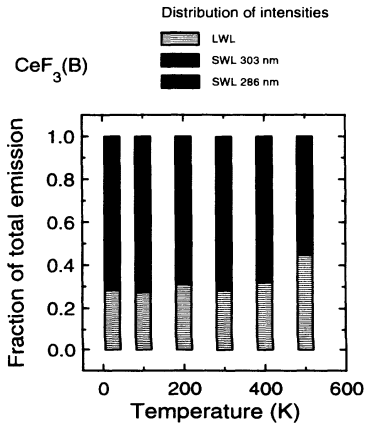

FIG. 4. The distribution of the total emission from the sample *B* (CeF_3) between three bands (SWL) bands peaking at 286 and 303 nm, and LWL band at 340 nm) for different temperatures.

TABLE I. Gaussian decomposition of emission spectra. Parameters of the Gaussian curves used to fit the steady state Ce emission spectrum in CeF_3 (sample *B*) and LaF_3:Ce (sample *H*), excited at 250 nm. The peak amplitudes of the 303 nm (for sample *B*) or 286 nm (for sample *H*) emission bands were normalized to unity. FWHM is the full width at half maximum.

Emission/ sample/ temperature	Peak amplitude	FWHM (cm^{-1})	Peak position (cm^{-1})
286 nm/*B*/24 K	0.74	1520	34 970
303 nm/*B*/24 K	1.00	1520	32 890
286 nm/*H*/24 K	1.00	1520	35 026
303 nm/*H*/24 K	0.79	1520	32 949
286 nm/*B*/300 K	0.24	1500	34 600
303 nm/*B*/300 K	1.00	2200	32 890
286 nm/*B*/500 K	0		
303 nm/*B*/500 K	1.00	2500	32 890

transfers from the regular Ce ions to the Ce_{per} ions. We will discuss this problem in Secs. III D and IV A. The second band in the excitation spectrum of the LWL coincides with the characteristic band of the SWL spectrum (two upper traces) as observed before.[17,22,16]

In interpreting excitation spectra we would like to introduce a note of caution. There are reasons to suspect that the excitation spectra of Fig. 5 (especially the two upper traces) may be distorted by a trivial optical effect that we have repeatedly observed:[18] Whenever the absorption coefficient is large, as in the case of concentrated Ce compounds, the maxima in the excitation spectrum may be replaced by minima giving appearance of "splitting." These distortions arise solely from the details of imaging of the emitting volume on the slit of the monochromator[32] and should not be interpreted in terms of real physical effects. They can be minimized by minimizing the total excited volume, e.g., by using thin samples or by using samples with lower concentrations of Ce. To achieve this the SWL excitation spectrum was repeated for the nominally undoped LaF_3 sample (sample *H*) and is shown as the upper trace of Fig. 6. Notice that the position of the characteristic band (249 nm) is shifted toward shorter wavelengths, indicating a lower distortion. The excitation spectrum of the LWL in this sample (not shown) is identical to that of the SWL (no characteristic band at 268 nm). This observation confirms earlier reports.[16,22] The most likely explanation is that for lower concentrations of the LWL centers most of the energy that they receive reaches them by the energy transfer from the SWL centers rather then by direct absorption.

With some precautions a good, presumably undistorted, excitation spectrum of the LWL band can be obtained also on the fully concentrated CeF_3 sample simply because the concentration of Ce_{per} is often sufficiently low to avoid distortions. The lower trace of Fig. 6 gives such an example indicating that the peak of the characteristic band in the excitation spectrum of the LWL is 268 nm. The dashed lines in Fig. 6 present Gaussian fits which will be used in the energy-transfer calculations.

It is possible to completely avoid the aforementioned distortions, even in concentrated and thick samples, by minimizing the excited volume. An example is shown in Fig. 7, which presents the spectrum taken at the Brookhaven Light Source for the CeF_3 sample (*B*) at about 300 K (RT). We see there, that the dominant band is located at 249 nm in agreement with the upper trace of Fig. 6 and, in addition, there are three more bands. Five bands due to the split levels of the Ce^{3+} *d* configuration were observed before.[16,22] The fifth band peaks below 200 nm and could not be observed in our experiment.

Table II summarizes the results of decomposition of excitation spectra into Gaussian curves. Although there are some differences in widths (probably due to the thermal broadening), the Gaussian components obtained from the spectra of the diluted and concentrated Ce samples (Figs. 6 and 7) are reasonably consistent.

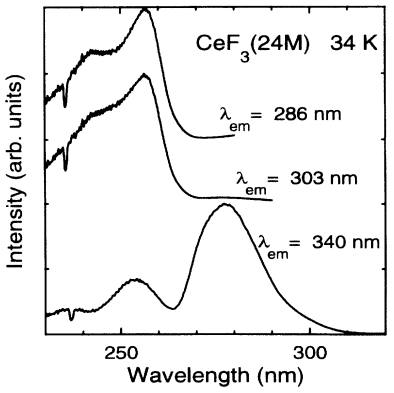

FIG. 5. Excitation spectra of the three emission bands from the sample 24*M* (CeF_3) at 34 K.

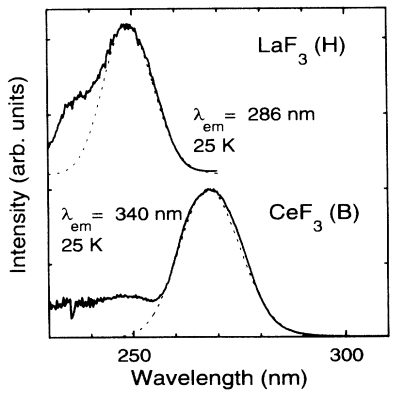

FIG. 6. Undistorted excitation spectra of SWL and LWL emissions. Upper trace presents the excitation spectrum of the 286-nm emission from the nominally undoped sample of LaF_3 (sample *H*) at 25 K. The lower trace presents excitation spectrum of the 340-nm emission at 25 K, sample *B* (CeF_3). Gaussian functions, fitted to the lowest energy characteristic bands, are shown by dashed lines.

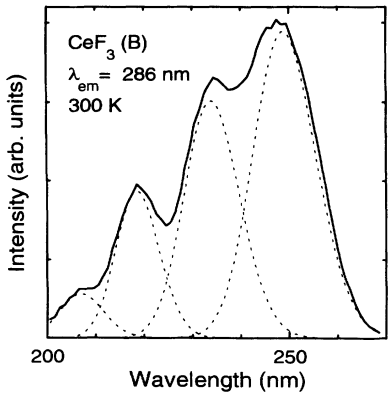

FIG. 7. Excitation spectrum of the 286-nm emission from sample *B* (CeF_3) at room temperature under synchrotron radiation (National Synchrotron Light Source at Brookhaven). Dashed lines present Gaussian components corresponding to transitions to different *d* levels of the excited Ce^{3+} ion.

C. Luminescence pulse shapes

In Fig. 8 we present optically excited (250 nm) pulse shapes for the SWL (trace *a*) and LWL (trace *b*) bands of the nominally undoped LaF_3 (sample *H*). Note the single-exponential decay of the SWL in the sample *H*. The pulse shape of the LWL in the 5% LaF_3:Ce shows a finite rise time, indicating that there is a transfer of excitation to the LWL emitters. The pulse shapes shown in Fig. 9 were taken under identical conditions but on the fully concentrated sample *B*. The SWL pulse shape, Fig. 9(a), now shows the presence of the initial faster decay (ultrafast component), while the LWL pulse shape, Fig. 9(b), is characterized by a finite rise time, as previously. Pulse shapes shown in Figs. 8 and 9 were taken at Brookhaven and may be somewhat influenced by the finite duration of the optical pulse, (0.5 ns), distorting the ultrafast component, as well as the high repetition rate of the synchrotron, which prevents observation of long components. Figure 10 presents a set of pulse shapes taken under ionizing excitation for the sample 24*M*. The presence of the ultrafast component is evident both for the polychromatic detection [Fig. 10(a)] and in the SWL [Fig. 10(b)]. The slow rise time is present in the LWL pulse shape [Fig. 10(c)]. In Table III we summarize more results including also some other samples. The basic characteristics of pulse shapes are consistent with those reported before,[33,17] and can be summarized as follows:

TABLE II. Gaussian decomposition of the excitation spectra.

Sample/ emission/ temperature	Figure	Peak amplitude	FWHM (cm^{-1})	Peak position (cm^{-1})
B/SWL/300 K	7	1.0	2450	40 160
		0.73	2450	42 740
		0.38	2200	45 750
		0.12	2450	48 300
H/SWL/25 K	6	1.0	2200	40 160
B/LWL/25 K	6	1.0	2350	37 310

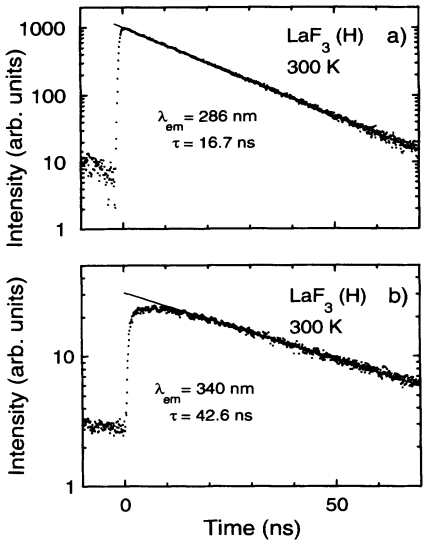

FIG. 8. Luminescence pulse shapes under pulsed synchrotron excitation at 250 nm at room temperature for different emission bands: (a) SWL band from the undoped LaF_3, sample *H*, (b) LWL band from the 5% Ce-doped LaF_3 (sample *J*). Straight lines show single-exponential fits, with decay times as indicated.

(1) The decays of SWL for two different types of excitations, optical (exciting light wavelength 250 nm), and ionizing (γ and β from the Ru/Rh radioactive source), are very similar, both indicating the presence of the ultrafast component. This result differs from a recently reported observation,[16] that the ultrafast component occurs only under ionizing excitation.

(2) Under ionizing excitation all decays show a slow component (200–400 ns) with a zero-time amplitude of

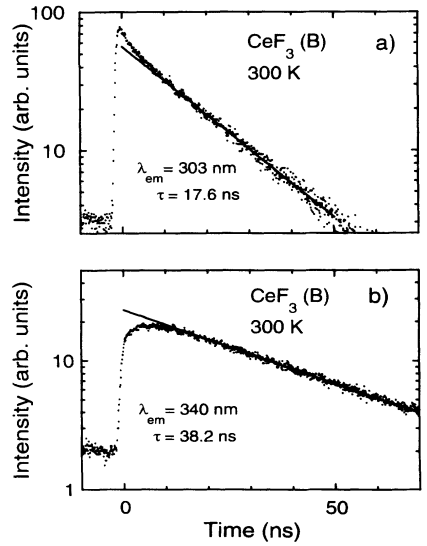

FIG. 9. Luminescence pulse shapes under pulsed synchrotron excitation at 250 nm at room temperature for different emission bands of CeF_3 (sample *B*): (a) SWL band (303 nm), (b) LWL band 340 nm. Straight lines present single-exponential fits, with decay times as indicated.

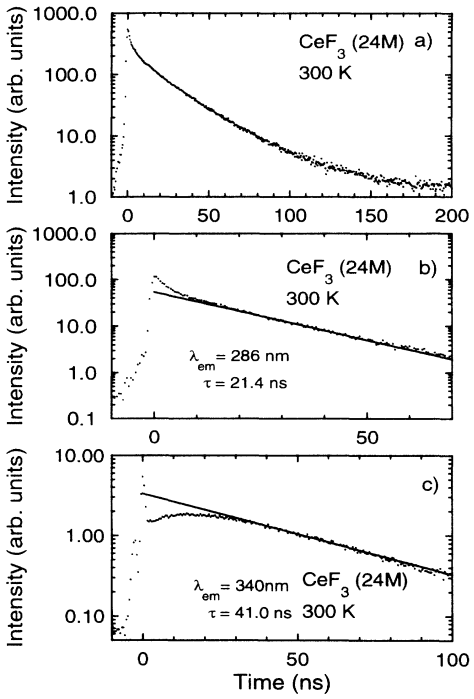

FIG. 10. Luminescence pulse shapes under ionizing excitation (γ and β, Ru/Rh source) for different emission bands from CeF_3 (sample 24*M*) at room temperature: (a) spectrally unresolved, polychromatic detection, (b) SWL band, and (c) LWL band. Solid lines present single-exponential fits with decay times as indicated.

about 0.5%.

(3) The two SWL bands display similar pulse shapes, characterized by a very short rise time and similar decay times. For low-Ce doping decays are single exponential, while for higher x (see the CeF_3 decay in Fig. 9), they are nonexponential and show an ultrafast component, 2–3 ns. After subtraction of the slow component and for delays longer than 20–30 ns the observed decays approach a single-exponential decay of about 20–23 ns.

(4) The LWL pulse shapes show a rise time of 10–15 ns under both optical and ionizing excitations and for longer delays approach a single-exponential decay of about 30–32 ns.

It is interesting to observe that samples showing less contribution from the "perturbed" sites (the LWL band) have longer decay times of the SWL (22–23 ns), and longer decay times of the LWL (40–44 ns). Samples showing greater contribution from the "perturbed" sites are characterized by shorter decay times of the SWL (16–18 ns) and shorter decay times of the LWL (32–33 ns). When concentration of perturbers increases the decay time of the SWL can only decrease and thus the longest observed decays (22–23 ns) provide the best estimate of the radiative lifetime. The decay time of the LWL is always governed by the larger of the transfer and radiative rate. Hence the best estimate of the radiative lifetime of the perturbed Ce is obtained from the shortest observed decays (32–33 ns).

TABLE III. Decay times of SWL and LWL emissions. The longest (for the SWL emission) and the shortest (for the LWL emission) decay times for different samples of $Ce_xLa_{1-x}F_3$ after subtraction of the slow component. The decay were measured at RT under ionizing (γ and β) and optical (250 and 270 nm) excitations. The decay time of the emission with no monochromator (unresolved) was obtained from the fit for delay times between 10 and 70 ns.

Sample/x/ excitation	SWL 286 nm	SWL 303 nm	LWL 340 nm	Unresolved
24*M*/1.0/γ,β	21.4	22.2	41.0	22.7
18*M*/1.0/γ,β	19.2	19.7	44.0	20.8
4*M*/0.1/γ,β	16.4	19.2	34.1	25.0
14*M*/0.5/γ,β				27.4
20*M*/0.5/γ,β	18.8	22.5	32.0	
5*M*/0.01/γ,β				24.3
B/1.0/γ,β		17.3	32.6	
B/1.0/250 nm		17.6	38.2	
H/undoped/250 nm		16.7	42.6	
J/0.05/270 nm	14.8	18.3	30.4	

D. Radiation trapping

There is no doubt that the presence of Ce_{per} gives rise to what can be termed radiation trapping (radiative energy transfer). This kind of trapping occurs when, after emission by a regular Ce ion, a real SWL photon does not leave the crystal but is absorbed by one of the Ce_{per} ions and, after some delay, is emitted again as an LWL photon. Since the probability of absorption by Ce_{per} is different for photons emitted in 286- and 303-nm bands this process is expected to cause a spillover of intensity from the SWL to LWL, with a change in relative intensities between the two SWL bands. A convincing illustration of this effect is provided by Fig. 3. The effect is stronger for higher temperatures because of the larger overlap between 286-nm emission (Ce) and 268-nm absorption (Ce_{per}) due to the thermal broadening. At the same time measured decay constants, shown in Fig. 11, increase with temperature until, for higher temperatures, thermal quenching brings them down again. This obser-

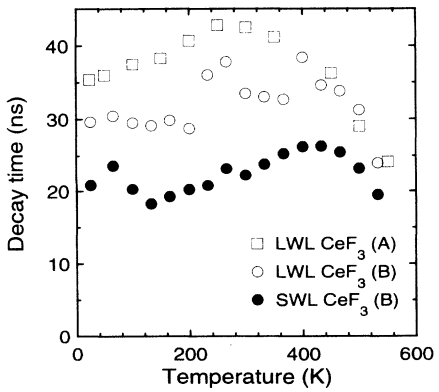

FIG. 11. Temperature dependence of decay times of the SWL and LWL under optical excitation at 270 nm for samples *A* and *B*.

vation can be explained to be a consequence of radiation trapping. As noted earlier,[34] when an average number of absorption-emission cycles $\langle n \rangle \leq 1.1$, the decay curve remains single exponential but the decay times change, depending on the path length and/or concentration of active centers. For higher $\langle n \rangle$ pulse shapes change qualitatively; they display apparent rise times and deviations from single-exponential form.[34] The correlation between changes in spectra and measured decay times was observed and interpreted in our work on Ce pentaphosphate.[18]

Figure 12 presents decay times of the LWL for sample B (a cube $10\times10\times10$ mm) and a small piece ($\sim1\times2\times2$ mm) of the CeF_3 crystal from the same boule. The decay times for the larger sample are significantly longer, indicating the radiation trapping. We want to emphasize that, to the extent that new crystals of CeF_3 (set M) are improved, showing no distortions of the SWL and lesser amounts of LWL, the effect of radiation trapping can be ignored. However, if much larger or lower quality crystals are to be used (e.g., in scintillation calorimetry), the problem may again require more attention.

E. Scintillation energy spectra

In Fig. 13 we show the energy spectrum produced by γ photons from the ^{207}Bi source interacting with CeF_3 [sample $3M'$, Fig. 13(a)] and BGO [Fig. 13(b)]. The energy spectrum represents the number of detected scintillators (Y axis) characterized by a specific amount of light (X axis) collected in some predetermined time (clipping time or shaping time) after one γ photon had deposited part (or all) of its energy in the detector material. Since photopeaks correspond to those events, in which the total energy of a γ photon has been deposited, it is possible to determine the absolute light output L (defined as the total number of scintillation photons produced per one MeV of γ-photon energy) by comparing the positions of photopeaks for a given material with those produced by γ photons from the same source in some known standard material, such as BGO. The light output of the CeF_3 sample shown in Fig. 13 is 55% of BGO, for which we assume, after Holl, Lorenz, and Mageras,[35] a light output of 8200 photons/MeV. Therefore the light output of the $3M'$ sample of CeF_3 is 4510 photons/MeV. This is, to our knowledge, the highest light output ever reported for CeF_3. However, it seems that higher light outputs of samples from the set M' are in large part due to higher concentrations of "perturbed" Ce. This, for reasons discussed earlier, is unacceptable in some important applications. We will discuss this problem later in Sec. IV.

In Fig. 14 we present experimental and calculated light outputs in photons/MeV vs concentration of Ce in

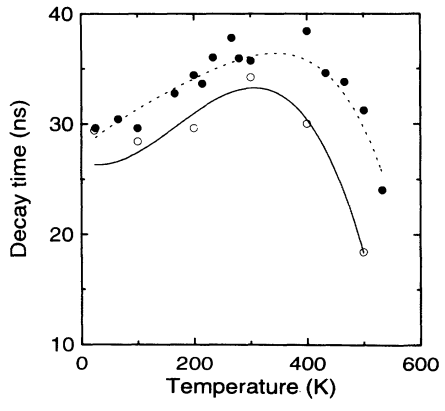

FIG. 12. Decay times of LWL at room temperature for two pieces of CeF_3 (sample B and B') under 270-nm excitation. Full circles present decay times measured for the larger, $10\times10\times10$ mm sample B; empty circles, for the smaller, $1\times2\times2$ mm sample B'.

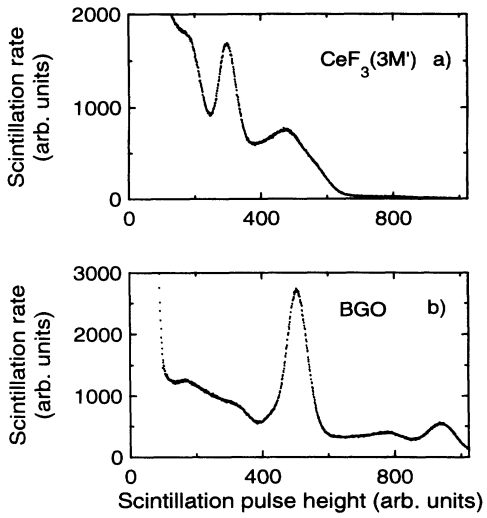

FIG. 13. Energy spectra generated by γ photons from the ^{207}Bi source, interacting with (a) CeF_3, sample $3M'$ and, (b) BGO.

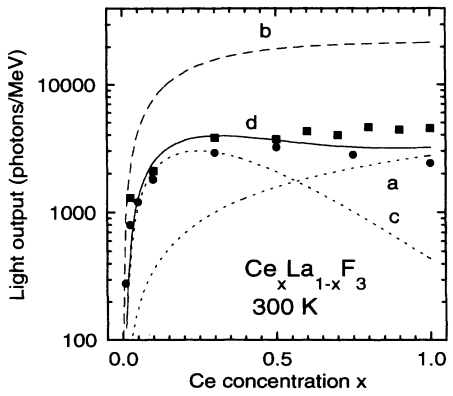

FIG. 14. The concentration dependence of the light output of $Ce_xLa_{1-x}F_3$ crystals (L vs x). Circles represent experimental data taken for samples from the set M; squares, data for the set M'. Solid and dashed lines indicate results of model calculations as explained in the text. (a) the light output due to direct excitation of Ce^{3+} ions; (b) the light output due to all three mechanisms, with no electron trapping; (c) the light output due to the mechanisms involving transfer from the lattice with electron trapping by Ce^{3+} ions; (d) the light output due to all three mechanisms, with electron trapping by Ce^{3+} ions.

$Ce_xLa_{1-x}F_3$ for samples of sets M and M'. The measured light output of samples from the set M' increases with x to a value of about 4500 (for $x > 0.6$). For set M it reaches maximum at $x = 0.5$ (about 3200) and then decreases to 2400 as x approaches unity. The solid and dashed lines present results of model calculations to be discussed in Sec. IV. Another quantity characterizing the scintillation process is the light output per ion (in photons cm^3/MeV/ion) defined as the light output divided by the number of Ce ions in one cm^3. In $Ce_xLa_{1-x}F_3$ the light output per ion decreases with increasing x, from the value of about 2×10^{-18} (for $x = 0.01$) to 2×10^{-19} (for $x = 1$).

It is instructive to compare the concentration dependence of the light output and light output per ion in $Ce_xLa_{1-x}F_3$ with those of other Ce-based scintillating materials. In $Ce_xLu_{1-x}PO_4$ the initial increase of the L with x is much sharper and saturation occurs for $x = 2\times10^{-3}$,[36] at the level very close to the conversion limited value of 18 700.[13] The light output per ion decreases from the value of about 1.2×10^{-15} for $x = 0.0005$ to the calculated value (under assumption of no quench for high-Ce concentration) of 1.3×10^{-18} for $x = 1$. In $Ce_xLa_{1-x}P_5O_{14}$ the light output is very nearly linear with x, approaching the value of about 4000,[18] much lower than the conversion limited value of 15 000.[13] Consequently, the light output per ion of about 1.1×10^{-18} is practically independent of x. Clearly, $Ce_xLa_{1-x}F_3$ represents an intermediate case, with much weaker but nevertheless distinct dependence of the light output per ion on the Ce concentration and much lower value of the total light output than the conversion determined limit.

IV. DISCUSSION

As described in the previous section the spectroscopy of the (Ce,La) trifluoride systems under optical and ionizing excitations provides a multitude of effects. Many of those effects have their origin in the presence of perturbed sites. Because of their unquestionable importance for the performance of the (Ce,La) trifluorides, they tend to overshadow the basic problem of scintillation mechanisms in the ideal lattice (with no perturbed sites). This problem must be addressed in order to make any meaningful assessment of the potential performance of improved (Ce,La) trifluorides as scintillation materials. Thus there are clearly two main themes running through this investigation.

We will address them separately in this section. In the first part of this section we will discuss the spectroscopy of (Ce,La) trifluorides with emphasis on the problem of perturbed Ce sites. The second part will be devoted to scintillation mechanisms in these materials.

A. Spectroscopy of $Ce_xLa_{1-x}F_3$

There is no crystallographic evidence of more than one R^{3+} site in the tysonite structure.[24] Yet the evidence is clear that there is more than one type of emission, (SWL and LWL), with different decay characteristics, (ultrafast component in SWL and slow rise time in LWL, also different radiative lifetimes), which implies more than one luminescent center. This observation had led us to the concept of "regular" (Ce^{3+}) and "perturbed" (Ce^{3+}_{per}) cerium ions,[17] later adopted and confirmed by other workers.[22,37] There are many indications, as described in more detail in the previous section, that there is a coupling between those two types of Ce ions, resulting in radiative and nonradiative energy transfer from Ce^{3+} to Ce^{3+}_{per} ions. While both transfers may produce slow rise times and nonexponential decays of the Ce^{3+}_{per} emission (LWL), the radiative transfer should also cause distortions in emission spectra of Ce^{3+} (SWL), as discussed before. The nonradiative energy transfer may be responsible for the nonexponential decays of the Ce^{3+} emission (SWL) and the slow rise time of the Ce^{3+}_{per} emission (LWL), although nonexponential decays induced by high density x-ray excitation have also been reported.[38] Both transfers may be responsible for the similarity between excitation spectra of two emissions (SWL and LWL).

Having already demonstrated that in new crystals of CeF_3 (set M) the radiative energy transfer has been substantially reduced (see Sec. III D), we will concentrate on the effect of the nonradiative energy transfer. From our analysis we will eventually estimate the fraction of perturbed Ce ions and will discuss the likely origin of "perturbers."

1. *Nonradiative Ce^{3+}-Ce^{3+}_{per} energy transfer*

We shall treat the problem of the nonradiative energy transfer utilizing the approach summarized in Ref. 39. First we have to introduce some conventions: Regular Ce^{3+} ions will be identified as donors (subscript d) and perturbed Ce^{3+} ions, (designated as C^{3+}_{per}) as acceptors, (subscript a). The theory adequately describing the nonradiative transfer between Ce^{3+} and Ce^{3+}_{per} ions is that of Inokuti and Hirayama, with no donor-donor energy migration. We will confirm this assumption for the Ce^{3+} ions in CeF_3 later, by explicit calculations of transfer rates between them. Since radiative transitions in both Ce^{3+} and Ce^{3+}_{per} are electric-dipole allowed, the donor-to-acceptor transfer rate is given by

$$W_{da} = \frac{\alpha_{da}}{R^6} \tag{2}$$

where α_{da} designates the transfer rate constant and R is the distance between donor and acceptor. The expression describing the decay of donor emission (Ce^{3+} emission, SWL) is given by

$$I(t) = I_0 \exp\left[\frac{t}{\tau_r} - \frac{4}{3}\pi^{3/2} n_a (\alpha_{da} t)^{1/2}\right], \tag{3}$$

where τ_r is the radiative lifetime of the donor emission and n_a is the concentration of acceptors (Ce^{3+}_{per}).[39] Equation (3) can be transformed to

$$y = ax^2 + bx + c, \tag{4}$$

by substituting $y = \log_e I(t)$, $x = t^{1/2}$, and a, b as in Eqs. (5) and (6), respectively,

$$a = -\frac{1}{\tau_r} \tag{5}$$

and

$$b = -\left[\frac{4}{3}\pi^{3/2} n_a (\alpha_{da})^{1/2}\right] . \tag{6}$$

Equation (4) is particularly useful for fitting the experimental (decay) data to a second-order polynomial as shown in Fig. 15. The figure shows experimental points and theoretical curves (solid lines) for two samples, *B* and 24*M*. It is worth noting that solid lines reproduce reasonably well experimental decays. The results of fits are as follows:

sample 24*M*, $a = -0.0421$ ns^{-1}, $b = -0.140$ ns$^{-1/2}$, $c = 4.594$,

sample *B*, $a = -0.0263$ ns^{-1}, $b = -0.295$ ns$^{-1/2}$, $c = 2.222$.

Radiative lifetimes for samples 23*M* and *B* are, from (5), 23.8 and 38.1 ns. We note that sample *B* shows strong effects of radiation trapping therefore we assume that the radiative lifetime of the Ce emission in (Ce,La) trifluorides is 23.8 ns, which is consistent with approximate estimates based on decay measurements. To make use of (6) and find the concentration of Ce^{3+}_{per}, n_a, we need an estimate of α_{da}, which is given by

$$\alpha_{da} = \left[\frac{1}{4\pi\varepsilon_0}\right]^2 \frac{3\pi\hbar e^4}{n^4 m^2 \omega^2} f_d f_a \int g_d(E) g_a(E) dE , \tag{7}$$

where m and e are electron mass and charge, ω is an average frequency of transitions involved in the transfer process, f_d and f_a are oscillator strengths of the d-f transition (emission) on the Ce^{3+} ion and f-d transition (absorption) on the Ce^{3+}_{per} ion, respectively, and $g_d(E)$ and $g_a(E)$ are normalized line-shape functions of the relevant transitions. It is clear that to use Eq. (7) we need the oscillator strengths of transitions under consideration.

2. *Oscillator strengths*

In our approach we will calculate oscillator strengths of relevant transitions from emission using a relation between the Einstein coefficient A, the inverse of the radiative lifetime τ_r, and the oscillator strength f. For the simple case of transition between two nondegenerate states (Kramers' doublets), the coefficient A can be expressed as

$$A = \frac{1}{\tau_r} = \frac{1}{4\pi\varepsilon_0} \frac{2\omega^2 e^2}{mc^3} \left[\frac{E_{loc}}{E}\right]^2 nf , \tag{8}$$

where m and e are electron mass and charge, c is the velocity of light, n is the refractive index, ω is the angular frequency of a transition and $(E_{loc}/E)^2 = (n^2+2)^2/9$ is the local-field correction.[39] For a transition connecting two sets of states, Eq. (8) will be replaced by

$$A_{tot} = \sum_i{}' \sum_j \frac{1}{4\pi\varepsilon_0} \frac{2\omega_{ij}^2 e^2}{mc^3} \left[\frac{E_{loc}}{E}\right]^2 nf_{ij} , \tag{9}$$

where primed summation indicates thermal averaging over the initial states, the second summation over the final states, ω_{ij} and f_{ij} are the angular frequencies and oscillator strengths of transitions connecting two states i and j. In the case of the Ce^{3+} ion the emitting transition connects one Kramers' doublet of the crystal-field split d^1 configuration ($i = 1$) with seven Kramers' doublets of the f^1 configuration ($j = 1,2,\ldots,7$).[40] Three of those doublets have $J = \frac{5}{2}$ and belong to the 286-nm emission, while remaining four are due to the $J = \frac{7}{2}$ and belong to the 303-nm emission band. By converting frequency to wavelength, using the expression for the local-field correction and inserting numerical constants we obtain the following expression reasonably approximating Eq. (9) in the case of the d-f transition on the Ce^{3+} ion:

$$f_d = \sum_{j=1}^{7} f_{1j} = A_{tot} \left[\frac{n(n^2+2)^2}{1.35\times 10^5 \lambda^2}\right]^{-1} . \tag{10}$$

Inserting values for $A_{tot} = 1/\tau_r = 4.2\times 10^7$ s^{-1}, $\lambda = 295\times 10^{-9}$ m, and $n = 1.66$, we find $f_d = 13.1\times 10^{-3}$. Since all seven doublets belong to the same irreducible representation,[28] it is reasonable to assume that all f_{1j} oscillator strengths for transitions connecting them with the lowest level of the d^1 configuration are the same. Therefore the oscillator strength of the absorption, which connects two Kramers' doublets with $j = 1$ and $i = 1$ will have the value of $(13.1/7)\times 10^{-3} = 1.87\times 10^{-3}$. To compare this value to the value obtained directly from the absorption spectrum, we will apply the Gaussian band-shape approximation formula,[41] to the published absorp-

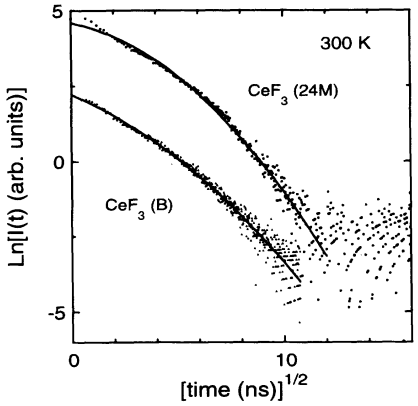

FIG. 15. Decays of the LWL bands from two samples of CeF_3 (24*M* and *B*). Points indicate experimental data taken at room temperature and under ionizing γ and β excitation (Ru/Rh source). Solid lines represent parabolic fits to the Inokuti-Hirayama theory, see text.

tion data:

$$f=\frac{1}{N}0.87\times10^{17}\frac{n}{(n^2+2)^2}\mu(\max)U\ , \tag{11}$$

where N is the concentration of the absorbing centers in cm^{-3}, n is the refractive index at maximum of the absorption curve, $\mu(\max)$ is the peak absorption coefficient in cm^{-1}, and U is the width of the absorption curve at half maximum in eV. Because of the large crystal-field splittings of d levels the final state is nondegenerate (transitions to different d levels are well separated) and we can assume that the absorption band at 250 nm is due to the $j=1$ to $i=1$ transition and that the oscillator strength $f=f_{11}$. Taking the data from Pedrini *et al.*,[22] $\mu(\max)=16\ cm^{-1}$, $U=0.176$ eV, $N=9.4\times10^{18}\ cm^3$, and the refractive index from the formula (1) ($n=1.656$) we obtain $f=1.92\times10^{-3}$, very close to our estimate based on the emission radiative lifetime (1.87×10^{-3}). Using this value and the excitation spectrum of Ce emission (Fig. 7, CeF_3, sample B), oscillator strengths for other absorption bands corresponding to transitions to higher d-levels were found and are presented in Table IV. The total f-d oscillator strength for four bands is 4.17×10^{-3}, significantly lower than the value given by Williams *et al.*[42] for Ce^{3+} in $LuPO_4$ (1.23×10^{-2}). The estimates of the oscillator strength for the 250-nm absorption band based on data of Elias *et al.*,[6] and Ehrlich, Moulton, and Osgood[7] and using Eq. (11), are 5.5×10^{-3} and 2.6×10^{-3}, respectively. It is important to note that our estimate based on the data of Pedrini *et al.*,[22] is consistent with the value calculated from emission decays which, being independent of Ce concentration, is likely to be the most reliable one.

For perturbed Ce^{3+} ions the same approach can be used to calculate the oscillator strength of the transition corresponding to the LWL emission band. Putting $A_{tot}=1/\tau_r=1/32$ ns$=3.13\times10^7\ s^{-1}$, the refractive index $n=1.64$ (at $\lambda=340$ nm) and $\lambda=340\times10^{-9}$ m into Eq. (10) we find $f=13.5\times10^{-3}$. Therefore $f_a=f/7=1.93\times10^{-3}$, reasonably close to the value that we have found for the Ce^{3+} ion (1.87×10^{-3} from emission and 1.92×10^{-3} from absorption). This result confirms the interpretation of the 340-nm emission as coming from the perturbed Ce ions. Since the symmetry of the regular Ce ion sites is already low we do not expect significant changes in transition-matrix elements, hence in oscillator strengths, after some additional perturbations are introduced. On the other hand it is reasonable to expect larger changes in transition energies because of the crystal-field sensitive d levels.

TABLE IV. Oscillator strengths of f-to-d transitions on the Ce^{3+} ion in LaF_3 at 300 K.

Peak position (cm^{-1})	Refractive index	Oscillator strength
40 160	1.656	1.92×10^{-3}
42 740	1.667	1.39×10^{-3}
45 750	1.679	0.64×10^{-3}
48 300	1.692	0.22×10^{-3}

3. *Nonradiative energy-transfer rates*

We are now in a position to calculate transfer rates using Eqs. (2) and (7) for all relevant cases, which are Ce^{3+}-Ce^{3+}, Ce^{3+}-Ce^{3+}_{per}, and Ce^{3+}_{per}-Ce^{3+}_{per}. To calculate appropriate overlap integrals we have used Gaussian functions found from decompositions of luminescence and excitation spectra and presented in Tables I and II. Some other constants used in these calculations are as follows: $f_d=13.1\times10^{-3}$, $f_a=1.93\times10^{-3}$, and $R=4.10$ Å. Transfer rates for the nearest neighbors [4.1 Å, (Ref. 24)] are (in s^{-1}): 7.70×10^5 for Ce^{3+}-Ce^{3+}, 1.56×10^9 for Ce^{3+}-Ce^{3+}_{per}, and 1.19×10^5 for Ce^{3+}_{per}-Ce^{3+}_{per}. All results are summarized in Table V. It is interesting to note that transfer rates between Ce^{3+}-Ce^{3+} and Ce^{3+}_{per}-Ce^{3+}_{per} are about 2–3 orders of magnitude lower than radiative transition rates ($\sim5\times10^7\ s^{-1}$). Therefore we do not expect any significant energy migration between excited Ce ions. Since, on the other hand, the Ce^{3+}-Ce^{3+}_{per} transfer rate is significantly higher than radiative transition rates we expect nonexponential decays of the Ce emission determined by concentration and distribution of perturbed Ce ions with no donor-donor energy migration as observed (see Fig. 15). The random distribution of acceptors (the continuum approximation), assumed in the Inokuti-Hirayama model, describes correctly the distribution of Ce^{3+}_{per} in CeF_3.

4. *Perturbed Ce^{3+} ions and "perturbers"*

Having derived a value α_{da} for the Ce^{3+}-Ce^{3+}_{per} transfer rate ($\alpha_{da}=W_{da}R^6=7.41\times10^{-36}\ cm^6/s$) we can use Eq. (6) to calculate n_a, the concentration of acceptors (Ce^{3+}_{per}) in two samples of CeF_3, B, and $24M$. We find

$$n_a(24M)=2.2\times10^{20}\ cm^{-3}\ (1.2\%)\ ,$$

$$n_a(B)=4.6\times10^{20}\ cm^{-3}\ (2.5\%)\ ,$$

which gives the probability P of Ce site not being per-

TABLE V. Some constants and results of calculations of overlap integrals and transfer rates.

	Ce-Ce	Ce-Ce*	Ce*-Ce*
Angular frequency ω at maximum overlap (s^{-1})	6.977×10^{15}	6.752×10^{15}	6.300×10^{15}
Refractive index n at maximum overlap	1.670	1.665	1.656
Overlap integral (J^{-1})	8.54×10^{13}	1.64×10^{18}	1.06×10^{14}
Transfer rate $W_{da}(s^{-1})$	7.70×10^5	1.56×10^9	1.19×10^5

turbed as 0.988 and 0.875 for samples 24*M* and *B*, respectively. Let us now assume that the source of perturbation originates in F^- sites (like vacancies or oxygen). A Ce ion, to be perturbed, needs only one of the nearest 11 surrounding F^- sites to be modified. Assuming that the probability of finding a perturber in one particular F^- site is ξ, we have the concentration of perturbers equal to $\xi 5.64\times10^{22}$ cm^{-3} and $P=(1-\xi)^{11}$. For sample 24*M*, $\xi=1.1\times10^{-3}$ (0.11%, 1100 ppm or 6.2×10^{19} perturbers/cm^3) and for sample *B*, $\xi=2.3\times10^{-3}$ (0.23%, 2300 ppm or 1.3×10^{20} perturbers/cm^3). For perturbation originating in Ce (La) site the values of perturber concentrations would be similar, since there are twelve cationic sites around each Ce ion.

At the present time there is no substantive model explaining the nature of perturbers. We can, however, eliminate a number of possibilities. First of all it would be highly unlikely for the perturbers to be cationic impurities. Absorption spectra taken at Optovac on very long crystals show no evidence of contamination, except for small amounts of other rare earths, principally Nd, in amounts of 10–100 ppm, significantly below our estimates. While, in principle, the presence of Nd^{3+} could cause some drainage of excitation by Ce-to-Nd energy transfer and reduce the light output, it is hard to explain how triply charged Nd ions would perturb Ce^{3+} ions to produce significant shifts of luminescence spectrum. Another possibility is the substitution of oxygen for fluorine. Since the charge state of oxygen is 2− (instead of 1 for fluorine), oxygen is clearly capable of perturbing neighboring Ce ions. However, resonance ionization spectroscopy performed by Atom Sciences Inc. on several of our CeF_3 samples from different crystal-growth runs, indicates an oxygen content of no more than 30–50 ppm. This is again significantly below our estimates. One must, therefore, conclude that the presence of oxygen alone cannot possibly account for the total concentration of perturbers.

We feel that the defect most likely to be involved in this perturbation is a fluorine ion vacancy. Clearly the presence of such a vacancy in the first coordinate sphere would markedly alter the crystal field influencing the Ce^{3+} ion. Such vacancies could be generated by a number of different mechanisms. First of all it is known that there is an intrinsic concentration of F^- vacancies in the tysonite structure, determined by conditions of crystal growth. These lattices show pronounced ionic conductivities, which have been attributed to the motion of F^- ions along one of their sublattices. From NMR experiments on LaF_3 it is known that at temperatures above 715 K intrinsic vacancies are formed by a Schottky process, whereas at lower temperatures they are ascribed to the presence of oxygen.[43] CeF_3 has a conductivity an order of magnitude higher than that of LaF_3 over a large range of temperatures,[44] which may indicate that vacancies form more readily in the Ce compound. It may be of further relevance that conductivity is increased in the presence of divalent cations, (Ba^{2+}, Sr^{2+}), which would enhance vacancy formation, whereas it is decreased in the presence of tetravalent impurities, (Th^{4+}), which would have the opposite effect.[44] These reported facts demonstrate the defect-prone characteristics of the tysonite lattice and may be involved in the generation of perturbed Ce sites.

B. Scintillation mechanisms in (Ce,La) trifluorides

In Sec. IV A we have discussed primarily the transfer processes that occur between luminescent centers, following a nonionizing, optical excitation. We will now concentrate our attention on those processes that precede the emission of visible photons after the material has been excited by a high-energy particle of a γ photon. Since this general subject has been treated by us in a recent publication[13] we will present it here only briefly.

It is convenient to divide the scintillation process into three consecutive steps: a conversion of the γ-particle energy into electronic-lattice excitations (electron-hole pairs and/or excitons), a transfer of the energy of these excitations to the emitting ion, and luminescence. These three processes can be described by the appropriately defined parameters (efficiencies), β,S,Q.[13] The overall scintillation efficiency η, is, therefore the product of the individual factors

$$\eta=\beta SQ, \quad 0\le\eta,\beta,S,Q\le1 , \tag{12}$$

where β, the efficiency of a conversion process, is determined by the fraction of the γ-photon energy lost to optical phonons,[13,45,46] S characterizes the transfer process,[13] and Q is the quantum efficiency of the luminescence center producing scintillation photons. Then the light output L (as defined in Sec. III E) can be expressed as

$$L=n_{\text{e-h}}\eta=\frac{10^6}{2.3E_g}\beta SQ , \tag{13}$$

where $n_{\text{e-h}}$ stands for the total number of electronic-lattice excitations which would be produced per one MeV of γ-photon energy if there were no losses to optical phonons, and E_g denotes the bandgap (in eV) of the material.[13] Since E_g and Q are usually known, L can be measured and β can be calculated using some material constants as described in Ref. 13, Eq. (13) can be used to calculate S, the transfer efficiency.

In Table VI we present parameters characterizing some Ce-based scintillator materials that we have studied recently (Refs. 13, 17, 18, 23, and 36). In Ref. 13 we discuss these and other materials in more details. Here we would like to point out that even a relatively low value of the conversion efficiency β (as in pentaphosphates and ultraphosphates) can be compensated by a high value of the transfer efficiency S. This is the case of $LuPO_4$:Ce, a scintillator characterized by a high light output, more than twice that of BGO. This result emphasizes the importance of the lattice-to-ion energy transfer and leads us to the consideration of mechanisms of transfer.

The well-known case in which lattice-to-ion transfer processes have been studied in detail is that of Tl-doped halides,[47] where the energy of e-h pairs is transferred to Tl^+ ions in a number of different ways. An important concept introduced in Ref. 47 and used to describe the contribution of the instantaneous transfer process is that of the characteristic volume (we will designate it V_c). It

TABLE VI. Characteristics of scintillator materials of interest. E_g—bandgap energy in eV; $n_{e\text{-}h}$—a total potential number of electron-hole pairs created per one MeV of γ-particle energy under assumption of no losses to optical phonons; L—light output in photons/MeV; η—total scintillation efficiency; β—conversion efficiency; Q—luminescence quantum efficiency; S—transfer efficiency.

Material	E_g	$n_{e\text{-}h}$	L	η	β	Q	S
CeP_5O_{14}	8.7	50 000	4000	0.08	0.30	1.0	0.27
$LuPO_4$:Ce	8.7	50 000	17200	0.34	0.37	1.0	0.92
CeF_3	10.4	42 000	2400	0.06	0.61	1.0	0.10
$Ce_{0.5}La_{0.5}F_3$	10.4	42 000	4500	0.11	0.61	1.0	0.18

is defined there as the volume from which the Tl^+ ion can gather holes. In NaI:Tl V_c was estimated to be about 27 unit cells,[47] being most likely determined by the band-like hot hole diffusion length. This diffusion length is determined by a random walk during which a hole loses its energy through longitudinal optical phonons ending up as a self-trapped hole (V_k center).[48] It is useful to extend the notion of V_c to other cases,[18] when the hole diffusion length is very short. Then other processes such as direct excitation and/or ionization of activating ions, nonradiative energy transfer from self-trapped excitons or diffusion of V_k centers may be responsible for the extent of the V_c.

In many cases the V_c can be determined from the dependence of the light output on the concentration of the emitting centers. Assuming that the saturation of the light output results from overlapping of V_c's due to different, competing ions, V_c would be inversely proportional to the concentration for which the light output reaches a saturation value.[18] To cover the range of V_c's observed in Ce containing materials we introduce three types of processes by which the absorption of the γ particle can result in the emission of Ce originating photons.

Process A—direct excitation

In this process Ce^{3+} ions are directly excited by inelastic collisions with secondaries (electrons and x rays, denoted e_s) the shower generated a high-energy γ particle

$$e_s + Ce^{3+} \rightarrow e_s + (Ce^{3+})^* ,$$

where $(Ce^{3+})^*$ denotes an excited Ce^{3+} ion, followed by emission of a scintillation photon

$$(Ce^{3+})^* \rightarrow Ce^{3+} + h\nu .$$

It is expected that V_c in this case will be small (less than a unit cell), delivering an appreciable light output only for high concentrations of Ce ions.

Process B—direct ionization

In this process Ce^{3+} ions are directly ionized by inelastic collisions with secondaries

$$e_s + Ce^{3+} \rightarrow Ce^{4+} + e_s + e_c ,$$

where e_c denotes a conduction-band electron coming from the Ce^{3+} ion, followed by an electron-capture process and formation of Ce^{3+}-bound exciton

$$Ce^{4+} + e_c \rightarrow Ce^{3+} \begin{bmatrix} e \\ h \end{bmatrix} ,$$

then by an energy transfer to the Ce^{3+} electronic structure

$$(Ce^{3+}) \begin{bmatrix} e \\ h \end{bmatrix} \rightarrow (Ce^{3+})^*$$

and, eventually, emission of a scintillation photon

$$(Ce^{3+})^* \rightarrow Ce^{3+} + h\nu .$$

This process, likewise the process A, is expected to be characterized by a small value of V_c.

Processes A and B result from direct excitation or ionization of the Ce ion, while lattice-to-ion energy transfer is absent. This is typical of Ce pentaphosphate,[18,23] where the low light output combined with lack of saturation even at the 100% Ce limit indicates a V_c much less than a unit cell.

However some other Ce containing materials (Ce:orthophosphates and Ce:orthosilicates) demonstrate high light outputs and saturations for concentrations as low as 0.1%, which indicates CV on the order of 1000 unit cells.[36,49] These observations clearly indicate that some long-range lattice-to-ion transfer processes must be active. Therefore we have to extend the list of possible processes leading to scintillation by including process C involving a lattice-to-ion energy transfer.

Process C—transfer from electronic-lattice excitations

In this process the energy of electron-hole pairs, e-h, is transferred to Ce ions either by consecutive trapping of charge carriers or by processes involving excitons ($\begin{smallmatrix} e \\ h \end{smallmatrix}$), free or self-trapped:

$$Ce^{3+} + e + h \rightarrow Ce^{4+}(Ce^{2+}) + e(h) \rightarrow (Ce^{3+})^*$$

or

$$Ce^{3+} + \begin{bmatrix} e \\ h \end{bmatrix} \rightarrow (Ce^{3+})^* .$$

In the next step a scintillation photon is emitted:

$$(Ce^{3+})^* \rightarrow Ce^{3+} + h\nu .$$

While in any particular case this process may involve both of the two options it is, nevertheless, possible to describe it in any case phenomenologically, by introducing V_c treated as an adjustable parameter.

It is obvious that contributions of the processes A and B, for lightly doped materials will be relatively unimpor-

tant, unless the process C is extremely inefficient. It is reasonable to expect that the light output due to these processes in $Ce_xLa_{1-x}F_3$ will be

$$L_{A+B}=n_{e\text{-}h}\beta\frac{x\omega_{Ce}}{x\omega_{Ce}+\omega_F} \tag{14}$$

where ω_{Ce}, ω_F denote probabilities of ionizing (or exciting) Ce^{3+} and F^- ions, respectively, by a shower of x rays or fast electrons induced by a γ particle and $n_{e\text{-}h}\beta$ is equal to the number of electronic excitations actually produced by a one MeV of a γ particle, since factor β takes into account a conversion loss due to phonons. Since there are three F^- ions for each Ce (La) ion it is reasonable to assume that $3\omega_{Ce}=\omega_F$.[23] Hence

$$L_{A+B}=n_{e\text{-}h}\beta\frac{x}{x+3}\ . \tag{15}$$

We also expect that $L_A=\varphi L_{A+B}$ for any x, since contributions of processes A and B, the probabilities of direct excitation and photoionization of Ce^{3+} ions should be in a constant ratio. Therefore

$$L_A=\varphi n_{e\text{-}h}\beta\frac{x}{x+3}\ . \tag{16}$$

Equation (16) was used to calculate the curve labeled (a) in Fig. 14, with $n_{e\text{-}h}\beta=25\,600$ and $\varphi=0.5$. We have used a similar formula for $Ce_xLa_{1-x}P_5O_{14}$.[23] It is clear that CeF_3 is inferior to CeP_5O_{14}, since the light output per ion is lower (compare 2×10^{-19} and 1.1×10^{-18} photons cm^3/MeV/ion) and, also, the transfer efficiency S is lower (see Table VI). We assume therefore, as suggested by Eq. (16), that this apparent inferiority of CeF_3 is due to the fact that in CeF_3 only process A is operational and process B is quenched in some manner. We will demonstrate later that this assumption is consistent with other experimental facts and will suggest the possible explanation of this quenching.

Let us consider what happens in the material where all three processes are active. If $x=n/N$, where n is the number of Ce ions, N is the number of Ce and La ions in a volume V in which the energy of a γ particle was deposited, then the total light output will be

$$L=L_{A+B}+\left[n_{e\text{-}h}-L_{A+B}\right]\frac{V_n}{V}\ , \tag{17}$$

where V_n is that part of the total volume V, from which n Ce ions are able to collect the energy deposited in the lattice. To take correctly into account an overlap between characteristic volumes of different ions we assume

$$\begin{aligned} V_1&=V_c\ ,\\ V_2&=V_1+\frac{V-V_1}{V}V_1,\ldots,\\ V_n&=V_{n-1}+\frac{V-V_{n-1}}{V}V_1\ . \end{aligned} \tag{18}$$

The recurrence stops when n exhausts all available Ce ions ($n=xN$) in volume V. Equations (15), (17), and (18) were used to calculate curve (b) in Fig. 14, assuming, as previously, that $n_{e\text{-}h}\beta=25\,600$. The characteristic volume V_c was taken as equal to the volume of four $Ce(La)F_3$ molecules which roughly corresponds to $\frac{2}{3}$ of the volume of the $Ce(La)F_3$ unit cell. Although curve (b) reproduces correctly the experimental results for low concentrations (below 5%) for higher concentrations the light outputs are grossly overestimated.

We are therefore led to believe that in $Ce_xLa_{1-x}F_3$ (for low concentrations of Ce) the transfer efficiency η is determined mostly by a limited (nevertheless operational) transfer of the excitation from the lattice, while for higher concentrations this transfer is suppressed and the process of direct excitation of Ce ions dominates. A similar conclusion can be drawn from excitation spectra of Moses *et al.*,[16] where the ratio of areas under bands due to the f-d and band-to-band transitions changes strongly between LaF_3:Ce and CeF_3.

It is interesting to inquire into the physical origin of this effect. The explanation we propose is based on the fact that in large band-gap materials the 2+ charge state of Ce ion may be metastable. Therefore Ce^{3+} ion could play two different roles as a luminescence center and the second of the electron trap. For higher concentrations of Ce the formation of Ce^{2+} could significantly delay formation of both lattice excitons and Ce-bound excitons thus effectively quenching the contributions of processes B and C to the fast component of the scintillation light. The similar effect (trapping of electrons by Tl^+ ions) is responsible for the loss in the "prompt" component of scintillation in Tl-doped materials.[47]

To describe an effect of the electron trapping by Ce^{3+} ions we will introduce an effective volume controlled by n Ce ions

$$V_n^{\text{eff}}=V_n-V_n^t \tag{19}$$

where

$$\begin{aligned} V_1^t&=\xi V_1\ ,\\ V_2^t&=V_1^t+\frac{V_n-V_1^t}{V_n}V_1^t,\ldots,\\ V_n^t&=V_{n-1}^t+\frac{V_n-V_{n-1}^t}{V_n}V_1^t\ . \end{aligned} \tag{20}$$

The parameter ξ is determined by the electron capture cross section σ and the characteristic volume V_1 of the Ce^{3+} ion ($\xi\sim\sigma^{3/2}/V_1$). It is reasonable to assume that $\xi\sim1$. As previously, we assume that

$$L_C=(n_{e\text{-}h}-L_{A+B})\frac{V_n^{\text{eff}}}{V}\ . \tag{21}$$

Equations (21), (20), and (19) were used to calculate curve (c) in Fig. 14, with all parameters the same as in previous calculations and with $\xi=0.9$. Curve (c) represents, therefore, a contribution of the process C quenched by electron traps. Curve (d) was obtained by summing of contributions shown separately by (a) and (c). The agreement with experiment is reasonable.

The stability of the Ce^{2+} charge state and, in consequence, the low transfer efficiency S is presumably due to

the higher band-gap energy of the La(Ce)F_3. For materials with lower bandgaps (like $LuPO_4$:Ce or $Ce_xLa_{1-x}P_5O_{14}$) the Ce^{2+} is not stable and there is no competition for conduction band electrons. Thus in $LuPO_4$:Ce we expect the process C (with a much larger V_c probably because of longer diffusion lengths of valence band holes or excitons) to dominate, while in $Ce_xLa_{1-x}P_5O_{14}$ the scintillation light will be due to processes A and B, the efficient transfer of the energy from process C being excluded for other reasons, such as large lattice relaxation.[18,23]

V. CONCLUSIONS

In this paper we have presented results of extensive studies on a large set of $Ce_xLa_{1-x}F_3$ crystals including older as well as recently grown samples. The significant progress made by Optovac in growing high-quality CeF_3 is quite evident. In samples grown several years ago the emission was dominated by LWL, attributable to what we have called perturbed Ce ions. Only at a high dilution ($<1\%$ Ce) was the normal Ce doublet (SWL) clearly visible.[6] Now the situation has changed and the SWL is dominant even in the fully concentrated material. The coupling between regular-regular Ce ions and regular-perturbed Ce ions (the later still present to some extent), has been treated by considering the nonradiative transfer. Using measured decays, calculated overlap integrals, an electric dipole-dipole transfer theory and a novel method for fitting data to the Inokuti-Hirayama theory, [Eqs. (4), (5), and (6)] we were able to obtain reliable data on radiative decay rates and transfer rates. This required also a thorough examination of values of oscillator strengths. Having all of these results we were able to use them in order to estimate the concentration of perturbers. Comparing these with measured concentrations of oxygen, we came to the conclusion that oxygen contamination is unlikely to account for the tenfold or larger concentrations of perturbers. The identity of perturbers still remains an open question, but the likelihood is that it is connected with native defects (fluorine vacancies) known to exist in the tysonite structure.

The scintillation properties of the fluoride have been treated by accounting for the efficiencies of conversion, transfer and luminescent emission. It became abundantly clear that the low efficiency of the lattice-to-ion transfer is responsible for the lower than predicted light output. As was discussed earlier,[13] an efficient transfer is needed to fully utilize conversion and can even go a long way to compensate for a poor conversion. Unfortunately in the case of CeF_3 inefficient transfer is truly limiting the overall efficiency of this scintillator.

The physical basis for a low transfer efficiency was examined by considering three different contributions (processes A, B, and C in Sec. IV B). We have shown that CeF_3 represents the worst case scenario because only process A, the direct excitation of the Ce ions contributes significantly to the scintillation.

Although some mixed (Ce,La) samples that exhibit substantial perturbed Ce emission have slightly higher light outputs, the defect-free CeF_3 presents the best hope for the fast and homogeneous scintillation material. Some increase of the light output (2 400–4 500 photons/MeV), due probably to slightly higher lattice-to-Ce_{per} energy transfer, is not enough to bring CeF_3 into the range of PET requirements, and may place some limits on the usefulness of this material for large calorimeter applications. As we have discussed in Sec. III D, the presence of perturbed Ce causes a radiative transfer (radiation trapping), which in large crystals may cause a size dependent lengthening of decay time, certainly a highly undesirable effect.

The most important conclusion of this work is that the negative effects observed in CeF_3 scintillators are not due to the high concentration of Ce, but to the presence of unwanted, perturbed Ce ions. Since there has been great progress in eliminating "perturbers" one can hope that further improvements in technology of CeF_3 will eventually produce a superior scintillation material for many applications in science and technology.

ACKNOWLEDGMENTS

We offer our special thanks to R. Sparrow and B. McCollum of Optovac Inc., North Brookfield, MA, who provided us with the samples of (Ce,La) trifluorides and took part in many fruitful discussions. Dr. C. Brecher and Dr. M. Weber have contributed extensively to the development of ideas and the form of their presentation. Dr. J. Sutherland has extended to us help and hospitality at the National Synchrotron Light Source in Brookhaven. One of us (M.B.) is grateful to the Kosciuszko Foundation for the financial support. Oxygen analysis was performed by Atom Sciences Inc. at Oak Ridge, Tennessee. The support of the Department of Energy under Grants No. DE-FG02-90ER61033 and DE-FG02-92-ER81360 is also gratefully acknowledged.

---

*On leave from Institute of Physics, N. Copernicus University, Torun, Poland.

[1]K. H. Butler, *Fluorescent Lamp Phosphors, Technology and Theory* (Pennsylvania State University Press, University Park, 1980), p. 258.

[2]P. F. Moulton, in *Lasers and Masers,* CRC Handbook of Laser Science and Technology, edited by M. J. Weber (CRC, Boca Raton, 1982), Vol. I.

[3]T. Hoshina, J. Phys. Soc. Jpn. **48**, 1261 (1980).

[4]Wm. S. Heaps, L. R. Elias, and W. M. Yen, Phys. Rev. B **13**, 94 (1976).

[5]A. Bril and H. A. Klasens, Philips Res. Rep. **7**, 421 (1952); G. Blasse and A. Bril, J. Chem. Phys. **47**, 5139 (1967).

[6]L. R. Elias, Wm. S. Heaps, and W. M. Yen, Phys. Rev. B **8**, 4989 (1973); K. H. Yang and J. A. DeLuca, Appl. Phys. Lett. **31**, 594 (1977).

[7]D. J. Ehrlich, P. F. Moulton, and R. M. Osgood, Jr., Optics Lett. **4**, 184 (1979); **5**, 339 (1980).

[8]P. Lecoq, in *Conference Record of the 1992 IEEE Nuclear Science Symposium and Medical Imaging Conference,* edited by F. Kirsten (IEEE, Piscataway, 1993), Vol. 1, p. 248; P. Lecoq, IEEE Trans. Nucl. Sci. **40**, 409 (1993); see also contributions of H. Newman, T. Matulewicz, H. Hilke, A. J. Dean, B. C. Grabmaier, and C. L. Melcher, in *Heavy Scintillators for Scientific and Industrial Applications,* Proceedings of the "Crystal 2000" International Workshop, edited by F. De Notaristefani, P. Lecoq, and M. Schneegans (Editions Frontières, Gif-sur-Yvette Cedex, France, 1993).

[9]R. Donaldson and M. G. D. Gilchriese, *Experiments, Detectors, and Experimental Areas for the Supercollider* (World Scientific, Singapore, 1988).

[10]D. Ferrere, M. Lebeau, M. Schneegans, M. Vivargent, and P. Lecoq, Nucl. Instrum. Methods Phys. Res. Sect. A **315**, 332 (1992); P. Lecoq, M. Schussler, and M. Schneegans, *ibid.* **315**, 337 (1992).

[11]S. E. Derenzo, W. W. Moses, J. L. Cahoon, T. A. DeVol, and L. A. Boatner, in *Conference Record of the 1991 IEEE Nuclear Science Symposium and Medical Imaging Conference,* edited by F. Kirsten (IEEE, Piscataway, 1991), Vol. 1, p. 143.

[12]G. Blasse, IEEE Trans. Nucl. Sci. **38**, 30 (1991).

[13]A. Lempicki, A. J. Wojtowicz, and E. Berman, Nucl. Instrum. Methods Phys. Res. Sect. A **333**, 304 (1993).

[14]K. H. Yang and J. A. DeLuca, Phys. Rev. B **17**, 4246 (1978).

[15]P. Dorenbos, C. W. E. van Eijk, R. W. Hollander, and P. Schotanus, IEEE Trans. Nucl. Sci. **37**, 119 (1990).

[16]W. W. Moses, S. E. Derenzo, M. J. Weber, F. Cerrina, and A. Ray-Chaudhuri, J. Lumin. (to be published).

[17]A. J. Wojtowicz, E. Berman, Cz. Koepke, and A. Lempicki, in *Conference Record of the 1991 IEEE Nuclear Science Symposium and Medical Imaging Conference* (Ref. 11), Vol. 1, p. 153; A. J. Wojtowicz, E. Berman, Cz. Koepke, and A. Lempicki, IEEE Trans. Nucl. Sci. **39**, 494 (1992).

[18]A. J. Wojtowicz, E. Berman, and A. Lempicki, IEEE Trans. Nucl. Sci. **39**, 1542 (1992).

[19]D. F. Anderson, IEEE Trans. Nucl. Sci. **NS-36**, 137 (1989).

[20]W. W. Moses and S. E. Derenzo, IEEE Trans. Nucl. Sci. **NS-36**, 173 (1989).

[21]D. F. Anderson, Nucl. Instrum. Methods Phys. Res. Sect. A **287**, 606 (1990).

[22]C. Pedrini, B. Moine, J. C. Gacon, and B. Jacquier, J. Phys.: Condens. Matter **4**, 5461 (1992).

[23]A. J. Wojtowicz, A. Lempicki, and E. Berman, in *Heavy Scintillators for Scientific and Industrial Applications* (Ref. 8).

[24]A. Zalkin, D. H. Templeton, and T. E. Hopkins, Inorg. Chem. **5**, 1466 (1966); A. K. Cheetham, B. E. F. Fender, H. Fuess, and A. F. Wright, Acta Crystallogr. B **32**, 94 (1976).

[25]C. G. Olson, M. Piacentini, and D. W. Lynch, Phys. Rev. B **18**, 5740 (1978).

[26]R. P. Lowndes, J. F. Parrish, and C. H. Perry, Phys. Rev. **182**, 913 (1969).

[27]R. Laiho and M. Lakkisto, Philos. Mag. B **48**, 203 (1983).

[28]All three (for $j=\frac{5}{2}$) and four (for $j=\frac{7}{2}$) Kramers doublets of the $Ce^{3+}f^1$ configurations ground state transform like $(\Gamma_3+\Gamma_4)$, see G. F. Koster, J. O. Dimmock, R. G. Wheeler, and H. Statz, *Properties of the Thirty-two Point Groups* (M.I.T., Cambridge, MA, 1963), p. 33.

[29]L. M. Bollinger and G. E. Thomas, Rev. Sci. Inst. **NS-32**, 1044 (1961).

[30]F. A. Kroger and J. Bakker, Physica **7**, 628 (1941).

[31]A. J. Wojtowicz, M. Kazmierczak, A. Lempicki, and R. H. Bartram, J. Opt. Soc. Am. B **6**, 1106 (1989).

[32]E. Berman, Ph.D. thesis, Boston University, Boston, 1992.

[33]W. W. Moses and S. E. Derenzo, Nucl. Instrum. Methods Phys. Res. Sect. A **299**, 51 (1990).

[34]Y. Sakai, M. Kawahigashi, T. Minami, T. Inoue, and S. Hirayama, J. Lumin. **41**, 317 (1989); R. Visser, P. Dorebos, C. W. E. van Eijk, A. Meijerink, G. Blasse, and H. W. den Hartog, J. Phys. Condens. Matter **5**, 1659 (1993).

[35]I. Holl, E. Lorenz, and G. Mageras, IEEE Trans. Nucl. Sci. **35**, 105 (1988).

[36]A. Lempicki, E. Berman, A. J. Wojtowicz, M. Balcerzyk, and L. A. Boatner, in *Conference Record of the 1992 IEEE Nuclear Science Symposium and Medical Imaging Conference* (Ref. 8), Vol. 1, p. 141; A. Lempicki, E. Berman, A. J. Wojtowicz, M. Balcerzyk, and L. A. Boatner, IEEE Trans. Nucl. Sci. **40**, 384 (1993).

[37]M. J. Weber, in *Heavy Scintillators for Scientific and Industrial Applications* (Ref. 8).

[38]C. Pedrini, B. Moine, D. Bouttet, A. N. Belsky, V. V. Mikhailin, A. N. Vasilev, and E. I. Zinin, Chem. Phys. Lett. **206**, 470 (1993).

[39]B. Henderson and G. F. Imbush, *Optical Spectroscopy of Inorganic Solids* (Clarendon, Oxford, 1989), p. 445.

[40]D. Piehler, Ph.D. thesis, University of California, Berkeley, 1990.

[41]D. L. Dexter, in *Advanced Solid State Physics,* edited by Seitz and Turnbull (Academic, New York, 1958), Vol. 6, p. 353.

[42]G. M. Williams, N. Edelstein, L.A. Boatner, and M. M. Abraham, Phys. Rev. B **40**, 4143 (1989).

[43]A. F. Aalders, A. F. M. Arts, and H. W. de Wijn, Phys. Rev. B **32**, 5412 (1985).

[44]A. Ross, M. Buijs, K. E. D. Wappenar, and J. Schoonman, J. Phys. Chem. Sol. **46**, 655 (1985).

[45]D. J. Robbins, J. Electrochem. Soc. **127**, 2694 (1980).

[46]W. van Roosbroeck, Phys. Rev. **139**, 1702 (1965).

[47]R. G. Kaufman, D. B. Hadley, and H. N. Harsh, IEEE Trans. Nucl. Sci. **17**, 82 (1970); H. B. Dietrich, A. E. Purdy, R. B. Murray, and R. T. Williams, Phys. Rev. B **8**, 5894 (1973).

[48]T. A. Green, M. E. Riley, P. M. Richards, G. M. Loubriel, and D. R. Jennison, Phys. Rev. B **39**, 5407 (1989).

[49]H. Suzuki, T. A. Tombrello, C. L. Melcher, and J. S. Schweitzer, Nucl. Instrum. Methods Phys. Res. Sect. A **320**, 263 (1992); C.L. Melcher and J. S. Schweitzer, *ibid.* **314**, 212 (1992).